RSC Advances

PAPER

View Article Online
View Journal | View Issue

Cite this: *RSC Adv.*, 2017, **7**, 51475

Theoretical study on the reaction mechanism of "ligandless" Ni-catalyzed hydrodesulfurization of aryl sulfide†

Sheng Fang, Meiyan Wang,* Jingjing Liu, Bingwen Li and Jing-yao Liu*

Received 28th September 2017
Accepted 29th October 2017

DOI: 10.1039/c7ra10755b

rsc.li/rsc-advances

The reaction mechanism of $Ni(COD)_2$ catalyzed hydrodesulfurization of aryl sulfide PhSMe with $HSiMe_3$ as the reducing agent has been studied by using density functional theory methods. Both PhSMe-coordinated pathway and "ligandless" pathway have been identified and compared. It is found that these two reaction pathways are kinetically competitive and the σ-complex assisted metathesis (σ-CAM) transition state is the highest point on each energy profile for both pathways. Moreover, both the singlet and triplet reaction pathways of ligand substitutions have been compared and found that both singlet and triplet reaction mechanisms are competitive for the ligand substitution of COD with PhSMe on PhSMe-coordinated pathway while the triplet mechanism holds a distinct advantage over singlet one for that of COD with $HSiMe_3$ on "ligandless" pathway.

Introduction

Ni catalysts, which are less toxic and less expensive comparatively, have spurred considerable interest in synthetic organic chemistry, particularly in activating chemical bonds, such as C–H,[1] C–C,[2] C–O,[3] C–N,[4] C–S,[5–8] and so on. Among all these bonds, the cleavage of C–S bonds has been less explored. Organosulfur compounds as electrophiles have been used in cross-coupling reactions to construct new C–C bonds.[5] Moreover, the cleavage of C–S bonds in organosulfur compounds makes extensive use of removal of blocking groups[6] and temporary directing groups.[7]

Hydrodesulfurization, *i.e.*, cleaving the C–S bond to form C–H bond, plays an importance role in manufacturing nonpolluting fuel from natural resources.[8,9] As early as 1940s, several Ni-mediated hydrodesulfurization reactions were reported with a large excess of Raney nickel as the reducing agent.[10] The homogeneous Ni-catalyzed hydrodesulfurization was carried out first by Wenkert and co-workers with stoichiometric amounts of highly reactive Grignard reagents possessing β-hydrogens as the reducing agent.[11] In 1999, Vicic and Jones found that the hydrodesulfurization of thiophene can be catalyzed by the nickel hydride dimer $[(dippe)NiH]_2$ with H_2 as the reducing agent.[12] Recently, silanes have been explored as the hydride source instead of H_2 in palladium,[13] rhodium[14] or nickel[15] catalyzed hydrodesulfurization of aryl sulfides. The $Ni(COD)_2$ (COD = (*Z*,*Z*)-1,5-cyclooctadiene) catalyzed reactions of aryl methyl thioethers (ArSMe) with dimethylethylsilane ($HSiMe_2Et$) have been presented by Martin and co-workers (Scheme 1). It is found that the reaction gives excellent chemselectivity under relatively mild reaction condition (90 °C), and especially the reaction can proceed under "ligandless" condition, *i.e.*, the typical σ-donor ancillary ligands such as phosphines are not present.[15]

By the experimental deuterium-labeling analysis,[15] the authors ruled out the possibility of *β*-H elimination and proposed a possible reaction mechanism, which consists of oxidative addition, metathesis and reductive elimination steps. However, the details of the reaction mechanism were not studied and some fundamental issues remain to be answered.[15] For example, although there are no σ-donor ancillary ligands under the reaction condition, the reactant ArSMe has the S atom, which can coordinate to the metal center to form σ-donor bond. As the bond dissociation energies of Ni ← C_2H_4 coordinate bonds[16] (34.3–41.2 kcal mol^{-1}) have been calculated to be a little higher than these of Ni ← S coordinate bonds[17] (25.2–37.0 kcal mol^{-1}), whether or not the reactant ArSMe replaces COD in $Ni(COD)_2$ acting as spectator ligand should be considered.

Laboratory of Theoretical and Computational Chemistry, Institute of Theoretical Chemistry, Jilin University, Changchun 130023, People's Republic of China. E-mail: ljy121@jlu.edu.cn

† Electronic supplementary information (ESI) available: Energy profiles of several secondary reaction pathways. Computation data of all transition states, minima and crossing points. Energy test of different post-HF and DFT methods. See DOI: 10.1039/c7ra10755b

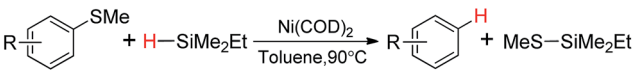

Scheme 1 $Ni(COD)_2$ catalyzed reaction of aryl methyl thioethers with dimethylethylsilane.

In this paper, the detailed reaction mechanism is investigated by using density functional theory (DFT) methods. To simplify the reaction, ArSMe and $HSiMe_2Et$ are modeled by PhSMe and $HSiMe_3$, respectively. The reaction pathways with or without PhSMe (*i.e.*, the "ligandless" one) as spectator ligand have been calculated and compared to figure out which one is preferred. As Ni(0)/Ni(II) and Ni(I)/Ni(III) catalytic cycles, which may include low spin and high spin species, are generally involved in nickel catalyzed reactions,[18] the different oxidation states and spin states of Ni are also considered. Hoping this theoretical study will give an insight into understanding the reaction mechanism of the "ligandless" reaction in detail.

Computational details

All calculations were performed with Gaussian09 package.[19] Molecular geometries of the model complexes were optimized without symmetry constraints *via* DFT calculations using B3LYP functional,[20] which has been shown to be adequate for studies of many nickel catalyzed reactions.[21] The Wachters-Hay basis set 6-311G[22] was used for Ni with an additional set of d polarization function, while all other main group atoms were described with 6-31G(d) basis set (the combination of the two basis sets is named as BSI). The ultrafine integration grid (99 590) was employed for making such optimizations more reliable. Frequencies calculations were carried out at the same level of theory to check all the optimized geometries as minima or transition states and to obtain zero point energy and thermal correction to free energies at 298.15 K and 1 atm. Intrinsic reaction coordinates (IRC) using the local quadratic approximation (LQA)[23] were calculated for each transition state to confirm the connecting of two relevant minima. To consider solvent effects, the single-point energy calculations for all the gas-phase optimized species were implemented at the level of ωB97XD functional[24] combined with a larger basis set 6-311++G(d,p) using the SMD model[25] in toluene. If not specifically pointed out, all energies during this article are based on the sum of Gibbs free energies of $Ni(COD)_2$ + 2PhSMe + $HSiMe_3$ in toluene solvent. Minimum energy crossing point (MECP) program[26] was applied to locate the crossing point between singlet and triplet species if necessary.

Results and discussion

Complex $Ni(COD)_2$ **1**, the precursor of catalyst in experiments,[15] has been calculated firstly and compared with the X-ray crystal structure (Fig. 1).[28] It is found that both the calculated bond distances of four coordination bonds and the two calculated bite angles of COD agree well with the experimentally measured parameters having the absolute differences within 0.013 Å and 0.4°, respectively, suggesting that the computational method is adequate to give the accurate molecular geometries.

To generate a vacant coordination site, one C=C double bond of a chelating COD ligand in **1** dissociates *via* transition state $\mathbf{TS_{1-2}}$ generating complex **2** with the C=C double bond dangling free (Fig. 2). The conformation of the non-chelating COD in **2** is twist-boat, same as in the Ni(0) complex observed by Tauchert *et al.* in experiment.[29] The coordination of thioether PhSMe and dissociation of non-chelating COD occur simultaneously through interchange mechanism *via* transition state $\mathbf{TS_{2-3}}$ to form complex **3**, in which PhSMe is coordianted to Ni with one double bond of benzene ring. $\mathbf{TS_{2-3}}$ is 23.2 kcal mol^{-1} higher than the reference point.

Oxidative addition of PhSMe to Ni(0) center proceeds *via* transition state $\mathbf{TS_{3-4}}$ leading to phenyl-Ni(II) thiolate complex **4** (Fig. 3), followed by the dissociation of one C=C bond of chelating COD through transition state $\mathbf{TS_{4-5A}}$ to give complex **5A**. In complex **5A**, the Ph group is *trans* to the vacant site due to its relatively strong *trans* influence. The overall energy barrier of oxidative addition of PhSMe is 26.3 kcal mol^{-1} relative to the reference point. In addition, replacing two COD ligands of **1** with two PhSMe molecules generating $Ni(PhSMe)_2$ **1T** has also been considered, it is found that the corresponding oxidative addition of PhSMe to $Ni(PhSMe)_2$ **1T** is not feasible kinetically (see Fig. S1 in ESI†).

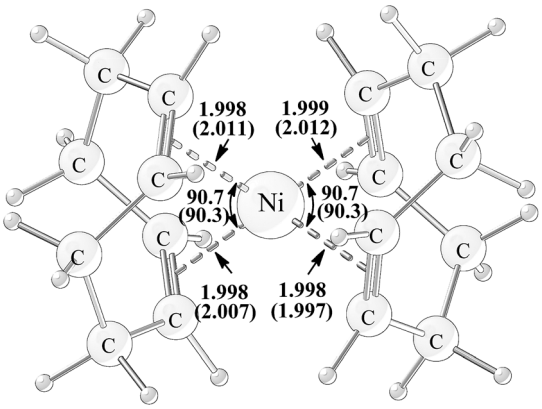

Fig. 1 Geometry structure of $Ni(COD)_2$ with the calculated and experimentally measured (in parentheses) bond distances (in unit of angstrom) and bite angles (in unit of degree).

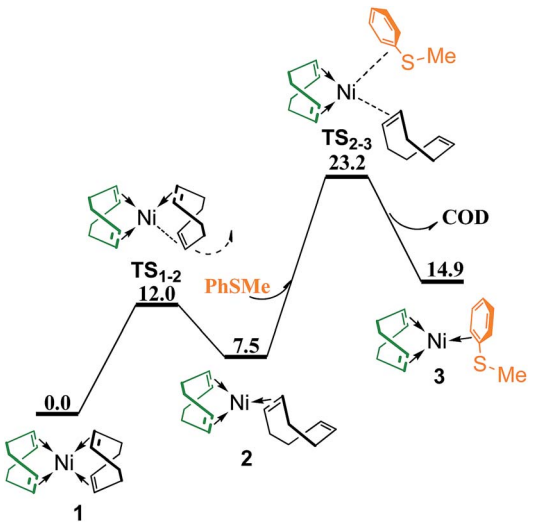

Fig. 2 Energy profile of ligand substitution of COD with PhSMe to give complex **3** (values are given in kcal mol^{-1}).

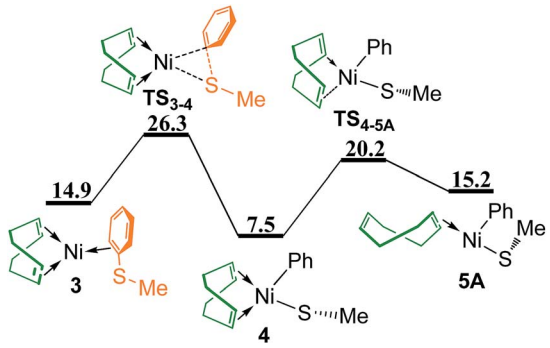

Fig. 3 Energy profile of oxidative addition and ligand dissociation to give complex **5A** (values are given in kcal mol^{-1}).

The silane $HSiMe_3$ coordinates directly to complex **5A** from the vacant site *via* $\mathbf{TS_{5A-6A}}$ giving complex **6A**, followed by σ-complex assisted metathesis (σ-CAM)[30] through $\mathbf{TS_{6A-7}}$ to generate complex **7** in which the formed (methylthio)trimethylsilane (Me_3SiSMe) is coordinated to Ni center (Fig. 4a). In Fig. 4b, isomerization of **5A** generates complex **5B** with the vacant site *trans* to the methylthio group (SMe). When $HSiMe_3$ coordinates to complex **5B** from the vacant site occurs *via* $\mathbf{TS_{5B-6B}}$ giving complex **6B**, from which the σ-CAM proceeds through $\mathbf{TS_{6B-8}}$ to release one benzene and generate complex **8** simultaneously. In addition, two other σ-CAM transition states are given in Fig. S2.† As these four corresponding σ-CAM transition states are higher than 35 kcal mol^{-1}, indicating that the σ-CAM process with COD coordinated to Ni is not kinetically feasible.

As mentioned in Introduction that the reactant thioether PhSMe may coordinate to Ni center to form σ-donor bond, the process involving thioether PhSMe substitution of COD are calculated and presented in Fig. 5. The coordination of PhSMe to complex **5A** proceeds *via* $\mathbf{TS_{5A-9A}}$ generating complex **9A**, followed by the dissociation of COD *via* $\mathbf{TS_{9A-10A}}$ giving complex **10A**. The isomerization of **5A** forms complex **5C**, from which the coordination of PhSMe and dissociation of COD can occur simultaneously through $\mathbf{TS_{5C-10B}}$ to generate complex **10B**, which is the isomer of **10A** (Fig. 5a). In Fig. 5b, the dissociation of COD from **5A** first proceeds *via* $\mathbf{TS_{5A-11}}$ forming complex **11**, then coordination of PhSMe occurs *via* $\mathbf{TS_{11-10A}}$ giving complex **10A**. Fig. 5c shows another reaction pathway to generate complex **10A**. Following the coordination of PhSMe from the site between Ph and COD *via* $\mathbf{TS_{5A-9B}}$ to give complex **9B**, the dissociation of COD proceeds *via* $\mathbf{TS_{9B-10A}}$ forming complex **10A**. Among the four pathways of replacing COD ligand with PhSMe, the last one, *i.e.*, **5A** → $\mathbf{TS_{5A-9B}}$ → **9B** → $\mathbf{TS_{9B-10A}}$ → **10A**, is most favorable as transition state $\mathbf{TS_{5A-9B}}$ is the lowest one.

From complex **10A** or **10B**, there are four reaction pathways involving σ-CAM processes to generate Me_3SiSMe or benzene (Fig. 6). The silane $HSiMe_3$ coordinates directly to complex **10B** from the vacant site *via* $\mathbf{TS_{10B-12A}}$ giving complex **12A**, followed by σ-CAM through $\mathbf{TS_{12A-13A}}$ to generate complex **13A** in which the formed Me_3SiSMe is coordinated to Ni center. Releasing Me_3SiSMe or PhSMe from metal center generates three-coordinated complex **14** or **15**. As **14** and **15** are higher than 35 kcal mol^{-1} in energy, indicating that the reaction pathways

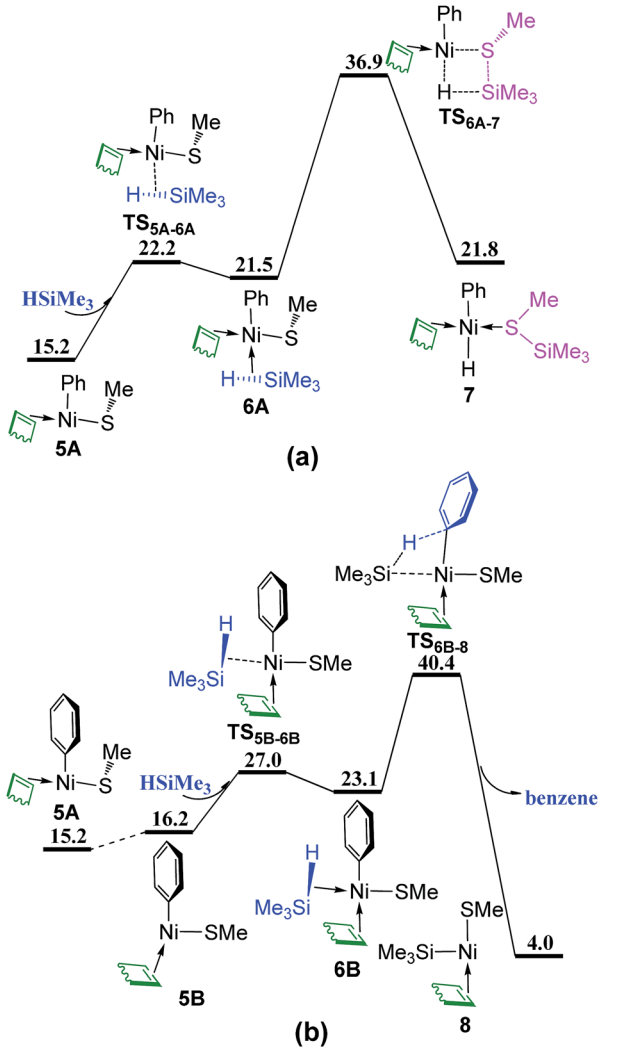

Fig. 4 Energy profiles of σ-CAM process from complex **5A** or **5B** with $HSiMe_3$: (a) coordination of $HSiMe_3$ directly to the vacant site; (b) coordination of $HSiMe_3$ from the site between COD and Ph (values are given in kcal mol^{-1}).

involving $\mathbf{TS_{12A-13A}}$ is not feasible thermodynamically (Fig. 6a). In Fig. 6b, $HSiMe_3$ coordination to complex **10A** from the site between PhSMe and Ph occurs *via* $\mathbf{TS_{10A-12B}}$ giving complex **12B**, from which the σ-CAM proceeds through $\mathbf{TS_{12B-16A}}$ to generate complex **16A** with benzene coordinated to Ni center. When $HSiMe_3$ coordinates to complex **10A** from the site between Ph and SMe, the reaction involves $\mathbf{TS_{10A-12C}}$ to give complex **12C**, followed by two σ-CAM *via* $\mathbf{TS_{12C-13B}}$ and $\mathbf{TS_{12C-16B}}$, respectively, to generate complexes **13B** and **16B**, with the formed Me_3SiSMe and benzene coordinated to Ni center (Fig. 6c). Since $\mathbf{TS_{12C-16B}}$ (Fig. 6c) is lower than $\mathbf{TS_{12C-13B}}$ (Fig. 6c) and $\mathbf{TS_{12B-16A}}$ (Fig. 6b) by 3.0 and 4.1 kcal mol^{-1}, respectively, the pathway involving $\mathbf{TS_{12C-16B}}$ to generate complex **16B** is most favorable.

Releasing benzene or PhSMe from complex **16B** occurs *via* $\mathbf{TS_{16B-17}}$ or $\mathbf{TS_{16B-18A}}$ forming three-coordinated complex **17** or **18A** (Fig. 7), followed by the corresponding reductive elimination through $\mathbf{TS_{17-19}}$ or $\mathbf{TS_{18A-20}}$ to generate complex **19** or **20**. The ligand substitution of PhSMe in **19** or benzene in **20** with

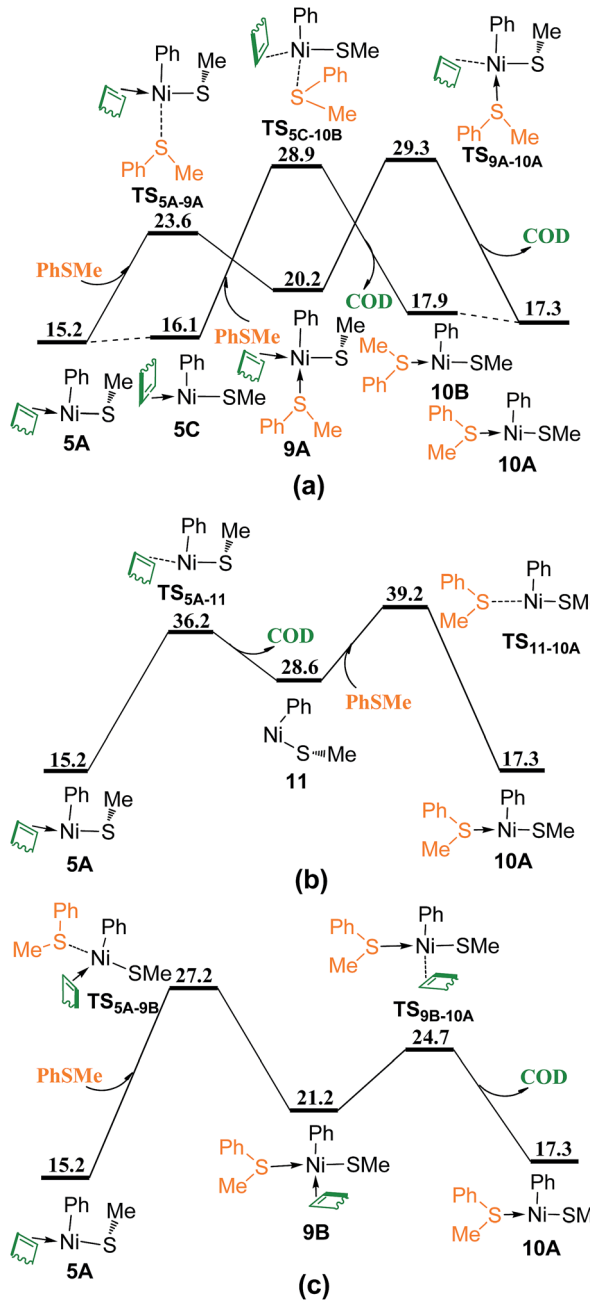

Fig. 5 Energy profiles of ligand substitution of COD with PhSMe: (a) coordination of PhSMe followed by dissociation of COD or simultaneously; (b) coordination of PhSMe following dissociation of COD; (c) coordination of PhSMe from the site between Ph and COD followed by dissociation of COD (values are given in kcal mol^{-1}).

COD ligand gives complex **21**, and subsequently ligand substitution of Me_3SiSMe with another COD regenerates complex $Ni(COD)_2$ **1**. Since the energy difference between $\mathbf{TS_{16B-17}}$ and $\mathbf{TS_{16B-18A}}$ is only 0.5 kcal mol^{-1}, in order to give more accurate comparison, the single-point energies for these two transition states were re-calculated at the ωB97XD/def2-QZVPPD level. It is found that $\mathbf{TS_{16B-17}}$ is only 0.1 kcal mol^{-1} lower than $\mathbf{TS_{16B-18A}}$. These results indicate that the dissociation of PhSMe or benzene ligand from **16B** occurs randomly.

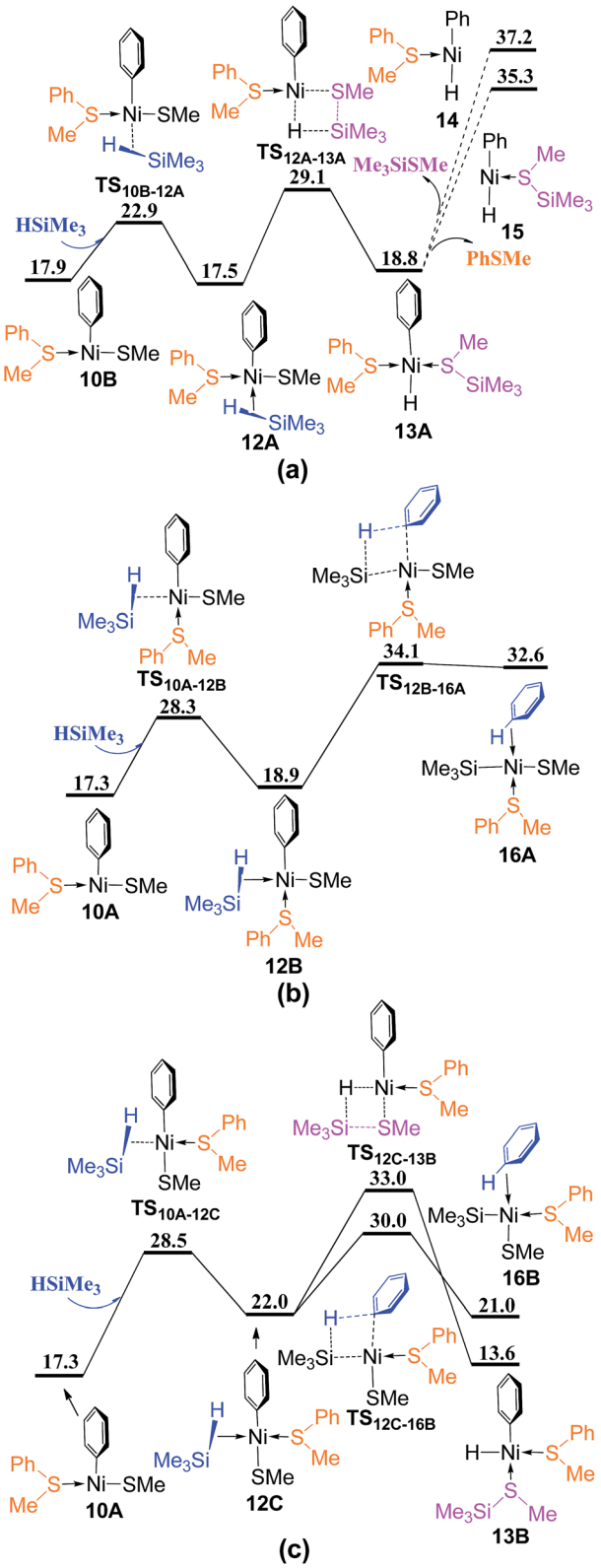

Fig. 6 Energy profiles of σ-CAM process from complex 10A or 10B with $HSiMe_3$: (a) coordination of $HSiMe_3$ directly to the vacant site; (b) coordination of $HSiMe_3$ from the site between PhSMe and Ph; (c) coordination of $HSiMe_3$ from the site between Ph and SMe (values are given in kcal mol^{-1}).

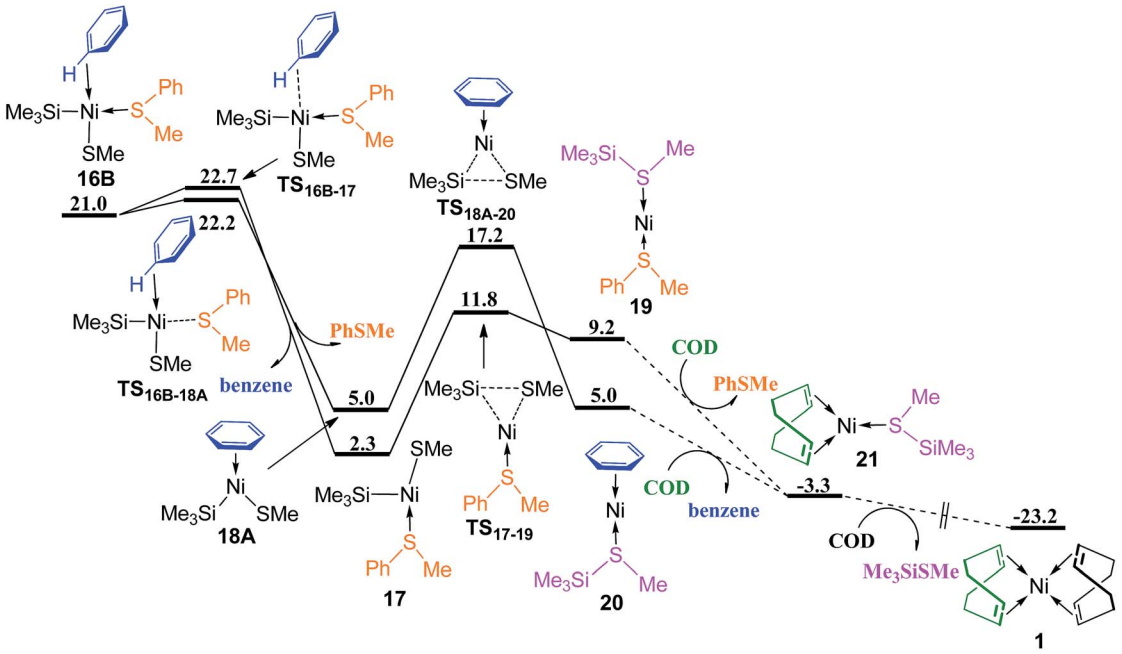

Fig. 7 Energy profiles of ligand substitution and reductive elimination to regenerate Ni(COD)$_2$ (values are given in kcal mol^{-1}).

The mechanism without COD ligand or PhSMe spectator ligand has also been considered. In Fig. 8, following the coordination of $HSiMe_3$ to the vacant site of three-coordinated complex **5A** *via* $\mathbf{TS_{5A-22}}$, the release of COD proceeds *via* $\mathbf{TS_{22-23A}}$ giving complex **23A**, in which an agostic interaction is formed. Isomerization of **23A** generates complex **23B** with the vacant site *trans* to Ph ligand. $\mathbf{TS_{22-23A}}$ (35.1 kcal mol^{-1}) is relatively high in energy, showing that this associated mechanism of ligand substitution is not favorable to form the complex without coordinated COD. Another reaction pathway to generate complex **23B** was found and presented in Fig. 9 involving several triplet transition states and intermediates. Complex **5A** first isomerizes to **5C** and then overcomes a crossing point **CP1** to form a triplet complex $\mathbf{5B^3}$ (Fig. 9a). The density functional ωB97XD has been proved to be appropriate to evaluate the energy of triplet species (see Table S1 in ESI†). **CP1** is 10.5 kcal mol^{-1} lower than $\mathbf{TS_{22-23A}}$ (Fig. 8), suggesting that the reaction prefers to involve the triplet species. Isomerization of $\mathbf{5B^3}$ gives $\mathbf{5A^3}$. Silane $HSiMe_3$ coordinates to $\mathbf{5A^3}$ *via* $\mathbf{TS^3_{5A-22A}}$ giving complex $\mathbf{22A^3}$ in which $HSiMe_3$ is weakly coordinated to Ni with relatively long Ni–H and Ni–Si bond distances of 2.28 and 3.58 Å, respectively, and COD is strongly coordinated to Ni with two relatively short Ni–C bond distances of 2.21 and 2.37 Å, respectively. Complex $\mathbf{22A^3}$ isomerizes *via* $\mathbf{TS^3_{22A-22B}}$ to form complex $\mathbf{22B^3}$, which has relatively short Ni–H and Ni–Si bond distances of 1.86 and 3.19 Å, as well as two relatively long Ni–C bond distances of 2.63 and 2.64 Å. Release of COD proceeds *via* $\mathbf{TS^3_{22B-23A}}$ giving complex $\mathbf{23A^3}$ (Fig. 9b). There is another pathway from $\mathbf{5A^3}$ to form complex $\mathbf{23A^3}$ (Fig. 9c). The dissociation of COD first proceeds *via* $\mathbf{TS^3_{5A-11}}$ forming complex $\mathbf{11^3}$, quasi-linear same as in $NiSAr_2$ (Ar = C_6H_3-2,6-(C_6H_2-2,4,6-*i*-Pr_3)$_2$) observed by Nguyen *et al.* in experiments,[30] then coordination of PhSMe occurs *via* $\mathbf{TS^3_{11-23A}}$ giving complex $\mathbf{23A^3}$. Isomerization of $\mathbf{23A^3}$ takes place to form complex $\mathbf{23B^3}$, which goes through a crossing point **CP2** to generate the singlet complex **23B** mentioned in Fig. 8. $\mathbf{TS^3_{5A-22A}}$, the most high point on this triplet reaction pathway **5A** → **5C** → **CP1** → $\mathbf{5B^3}$ → $\mathbf{5A^3}$ → $\mathbf{TS^3_{5A-22A}}$ → $\mathbf{22A^3}$ → $\mathbf{TS^3_{22A-22B}}$ → $\mathbf{22B^3}$ → $\mathbf{TS^3_{22B-23A}}$ → $\mathbf{23A^3}$ → $\mathbf{23B^3}$ → **CP2** → **23B** in Fig. 9, is 25.5 kcal mol^{-1} in energy, 9.6 kcal mol^{-1} lower than $\mathbf{TS_{22-23A}}$ on the corresponding singlet reaction pathway (Fig. 8), indicating that this reaction pathway involving a double spin-flip singlet → triplet → singlet is preferred kinetically. Similar double spin-flip course has been

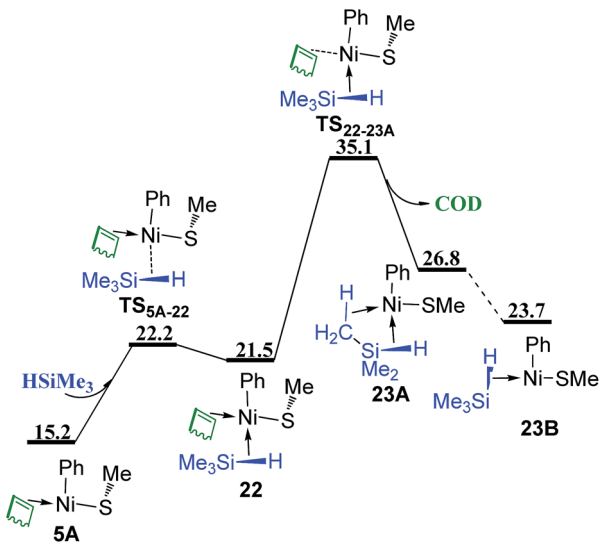

Fig. 8 Energy profile of ligand substitution of COD with $HSiMe_3$ (values are given in kcal mol^{-1}).

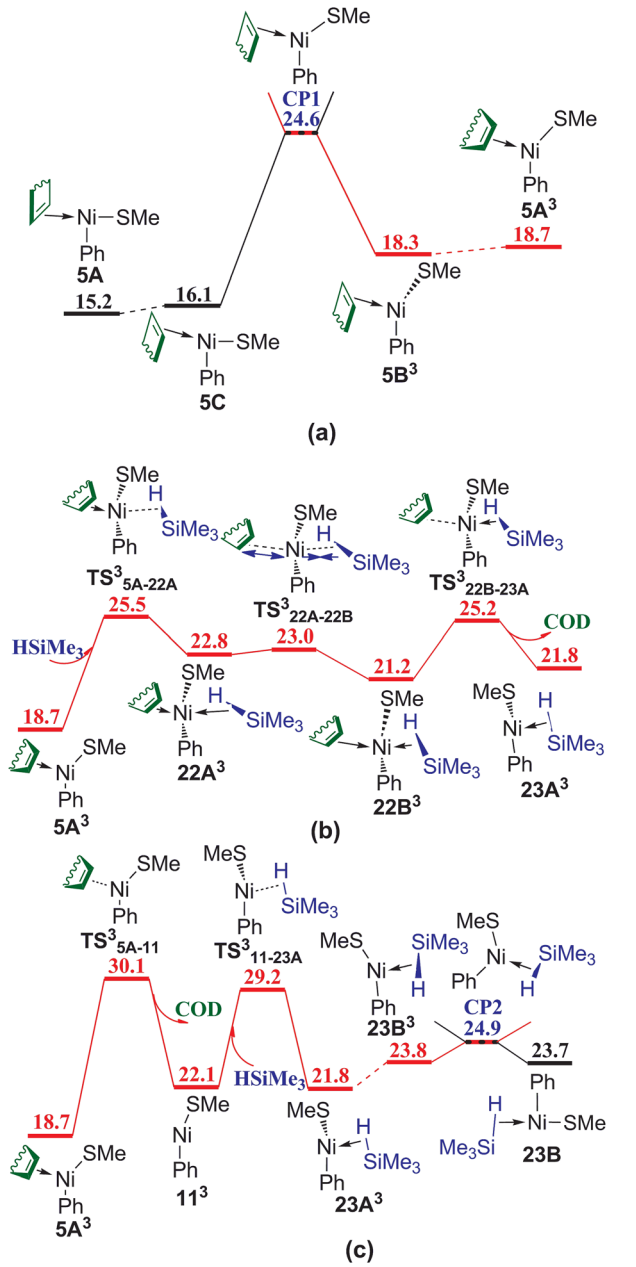

Fig. 9 Energy profiles of ligand substitution of COD with $HSiMe_3$ involving triplet species: (a) spin cross process from singlet state to triplet state; (b) triplet mechanism of ligand substitution of COD with $HSiMe_3$; (c) spin cross process from triplet state to singlet state (values are given in kcal mol^{-1}).

reported by Schlangen and Schwarz in computational study of $NiH^+ + CH_4 \rightarrow Ni(CH_3)^+ + H_2$ reaction.[31]

From complex **23B** (Fig. 10), the σ-CAM proceeds *via* $\mathbf{TS_{23B-18B}}$ and $\mathbf{TS_{23B-24}}$ to give complex **18B** and **24** with the formed benzene and Me_3SiSMe as ligand, respectively. $\mathbf{TS_{23B-18B}}$ is 6.2 kcal mol^{-1} lower than $\mathbf{TS_{23B-24}}$, showing that the σ-CAM process giving the benzene coordinated complex **18B** is preferred. Isomerization of **18B** generates complex **18A**, which has been mentioned in Fig. 7.

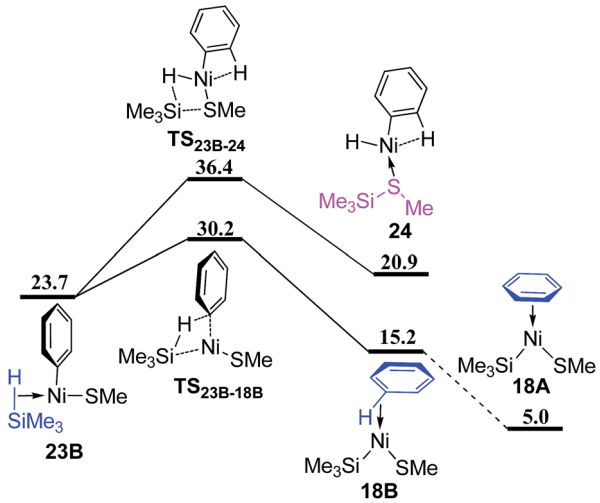

Fig. 10 Energy profiles of σ-CAM process from complex **23B** (values are given in kcal mol^{-1}).

Since the reaction pathway involving the triplet species has been found to be preferred for ligand substitution of COD in complex **5A** with $HSiMe_3$ to generate complex **23B** (Fig. 8 and 9), the corresponding triplet mechanism should be considered for ligand substitution of COD in complex **5A** with reactant PhSMe to give complex **10A**, the singlet pathway of which has been discussed in Fig. 5c. Isomerization of the triplet complex $\mathbf{5B^3}$ generated from the singlet complex **5A** through a crossing point **CP1** (Fig. 9a) forms complex $\mathbf{5C^3}$(Fig. 11). Coordination of PhSMe proceeds *via* $\mathbf{TS^3_{5C-9A}}$ forming complex $\mathbf{9A^3}$, subsequently isomerization of $\mathbf{9A^3}$ gives complex $\mathbf{9B^3}$, in which PhSMe is weakly coordinated with relatively long Ni–S bond distance of 2.577 Å, and COD is strongly coordinated with two relatively short Ni–C bonds of 2.265 and 2.425 Å, respectively. Complex $\mathbf{9B^3}$ isomerizes *via* $\mathbf{TS^3_{9B-9C}}$ giving complex $\mathbf{9C^3}$ which has relatively short Ni–S bond of 2.438 Å, and two relatively long Ni–C bonds of 2.651 and 2.641 Å. Release of COD proceeds *via* $\mathbf{TS^3_{9C-10}}$ giving complex $\mathbf{10^3}$, which can overcome a crossing point **CP3** (Fig. 12) to generate the singlet complex **10A** which has emerged in Fig. 5. Comparing the most favored singlet (Fig. 5c) and triplet (Fig. 9a, 11 and 12) reaction pathways, it is found that the highest singlet transition state $\mathbf{TS_{5A-9B}}$ (27.2 kcal mol^{-1} in Fig. 5c) is only 0.8 kcal mol^{-1} higher than the triplet one $\mathbf{TS^3_{5C-9A}}$ (26.4 kcal mol^{-1} in Fig. 11). In order to give more accurate comparison, the single-point energies for $\mathbf{TS_{5A-9B}}$ and $\mathbf{TS^3_{5C-9A}}$ were re-calculated at the ωB97XD/def2-QZVPPD level. It is found that $\mathbf{TS_{5A-9B}}$ is only 0.5 kcal mol^{-1} higher than $\mathbf{TS^3_{5C-9A}}$. These results indicate that the two reaction pathways are competitive with the triplet one slightly favored.

Besides the reactant PhSMe (Fig. 2), another reactant $HSiMe_3$ may also react first with complex **2** (Fig. 13). Oxidative addition of $HSiMe_3$ and dissociation of the dangling COD ligand from complex **2** proceed simultaneously *via* transition state $\mathbf{TS_{2-25}}$ giving complex **25**, from which one C=C bond of chelating COD dissociates through transition state $\mathbf{TS_{25-26}}$ forming complex **26**. The energy barrier of $\mathbf{TS_{25-26}}$ is 28.5 kcal mol^{-1}, still lower

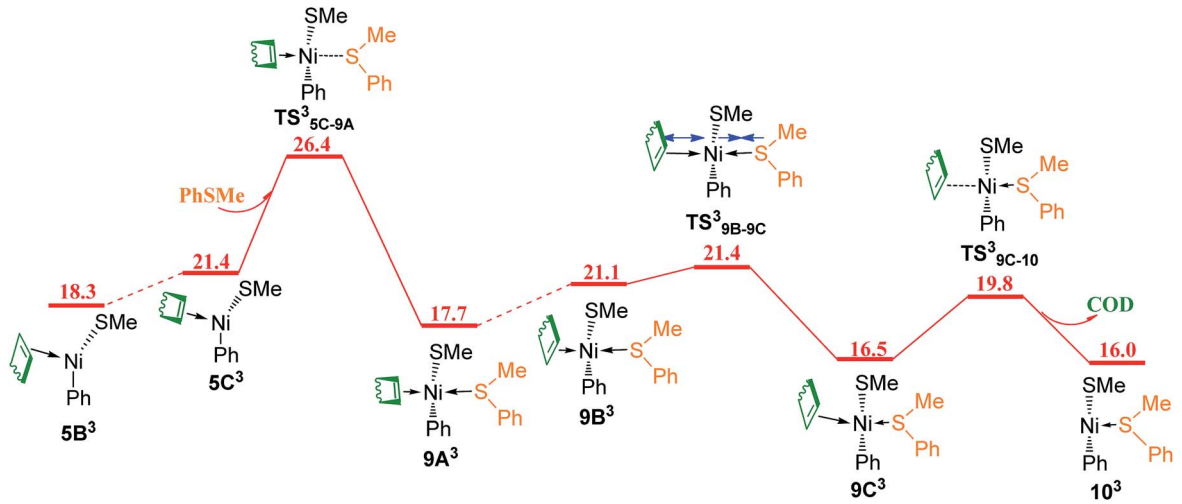

Fig. 11 Energy profile of triplet mechanism of ligand substitutions of COD with PhSMe (values are given in kcal mol^{-1}).

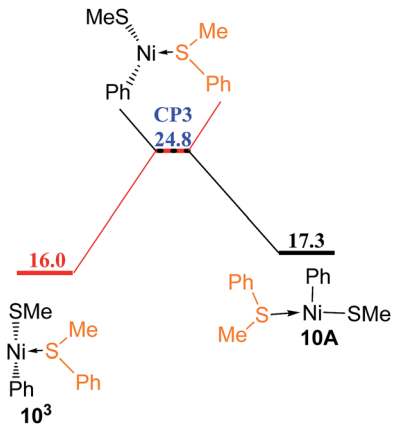

Fig. 12 Energy profile of spin cross process from triplet state to singlet state (values are given in kcal mol^{-1}).

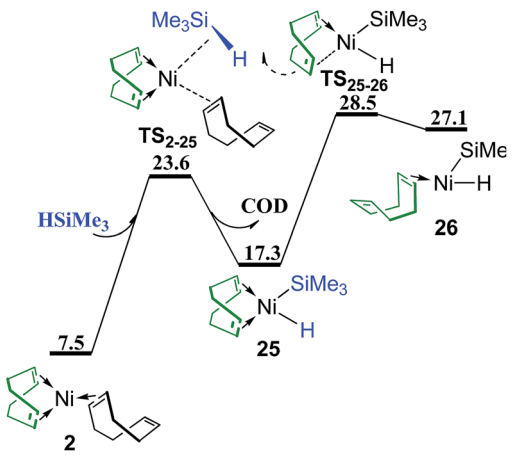

Fig. 13 Energy profile of ligand substitution of COD with $HSiMe_3$ and the oxidative addition of $HSiMe_3$ to give complex **26** (values are given in kcal mol^{-1}).

than $TS_{23B-18B}$ (30.2 kcal mol^{-1} in Fig. 10) and $TS_{12C-16B}$ (30.0 kcal mol^{-1} in Fig. 6c) which are involved in the reaction pathways when PhSMe reacts first with complex **2**. Thus, it is

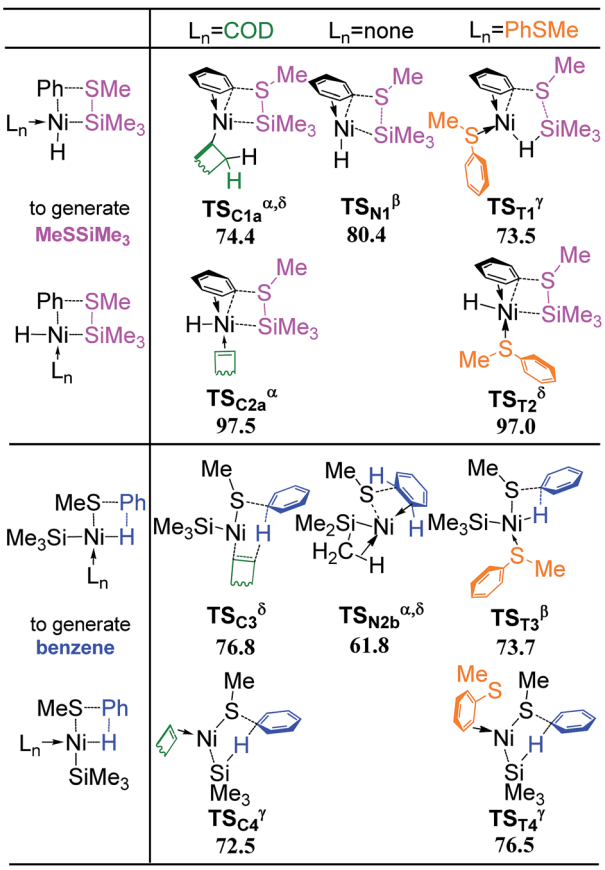

Scheme 2 Transition states of metathesis or quasi-metathesis processes from various Ni-hydride species with PhSMe. $^{\alpha}$Quasi-metathesis with two or more steps. $^{\beta}$Standard σ-metathesis. $^{\gamma}$Oxidative addition of $HSiMe_3$ occurs simultaneously. $^{\delta}$H atom of the Ni-hydride has to migrate to the COD ligand or the phenyl ring before this transition state (values are given in kcal mol^{-1}).

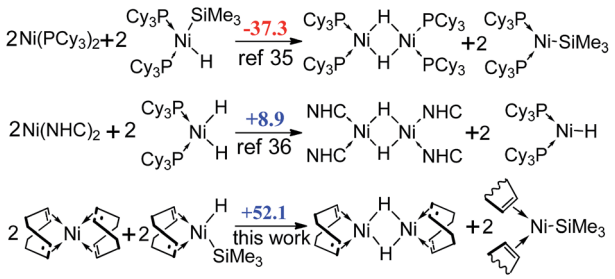

Scheme 3 The comparison of reaction free energies (ΔG^R, in kcal mol^{-1}) of the formation of dimeric Ni(I) complexes and Ni(I) radicals with two previous works.

necessary to consider the following metathesis steps. The corresponding transition states of metathesis or quasi-metathesis to generate Me_3SiSMe or benzene are listed in Scheme 2. Three situations of ligand (L_n) and the corresponding four topological orientations have been considered. It is found that all the transition states are higher than 60 kcal mol^{-1} in energy, indicating that all the reaction pathways following the reaction of $HSiMe_3$ with complex **2** are not feasible kinetically (see Fig. S3–S5† for details of these reactions).

In addition, since the formation of dimeric Ni(I) complex and Ni(I) radical (Scheme 3) has been demonstrated theoretically to be favored by using the phosphine ligand,[32] but not by using the NHC ligand,[33] we also calculated the reaction free energies for the formation of Ni(I) species with COD ligand. However, the reaction is 52.1 kcal mol^{-1} endergonic, showing that the Ni(I) species are thermodynamically unstable.

The overall catalytic cycles are presented in Fig. 14. The reaction mainly involves oxidative addition, ligand substitution, σ-CAM, reductive elimination and ligand substitution steps. For the first ligand substitution and σ-CAM steps, two reaction pathways, *i.e.*, the PhSMe-coordinated pathway and the "ligandless" pathway are involved having very small energy difference, only 0.2 kcal mol^{-1} between the rate-determining σ-CAM transition state **TS$_{12C-16B}$** (30.0 kcal mol^{-1} in Fig. 6c) in the former pathway and **TS$_{23B-18B}$** (30.2 kcal mol^{-1} in Fig. 10) in the latter one, indicating the two reaction pathways are competitive. The single-point energies of **TS$_{12C-16B}$** and **TS$_{23B-18B}$** were re-calculated at the ωB97XD/def2-QZVPPD level, and it is found that **TS$_{12C-16B}$** becomes slightly higher than **TS$_{23B-18B}$** by

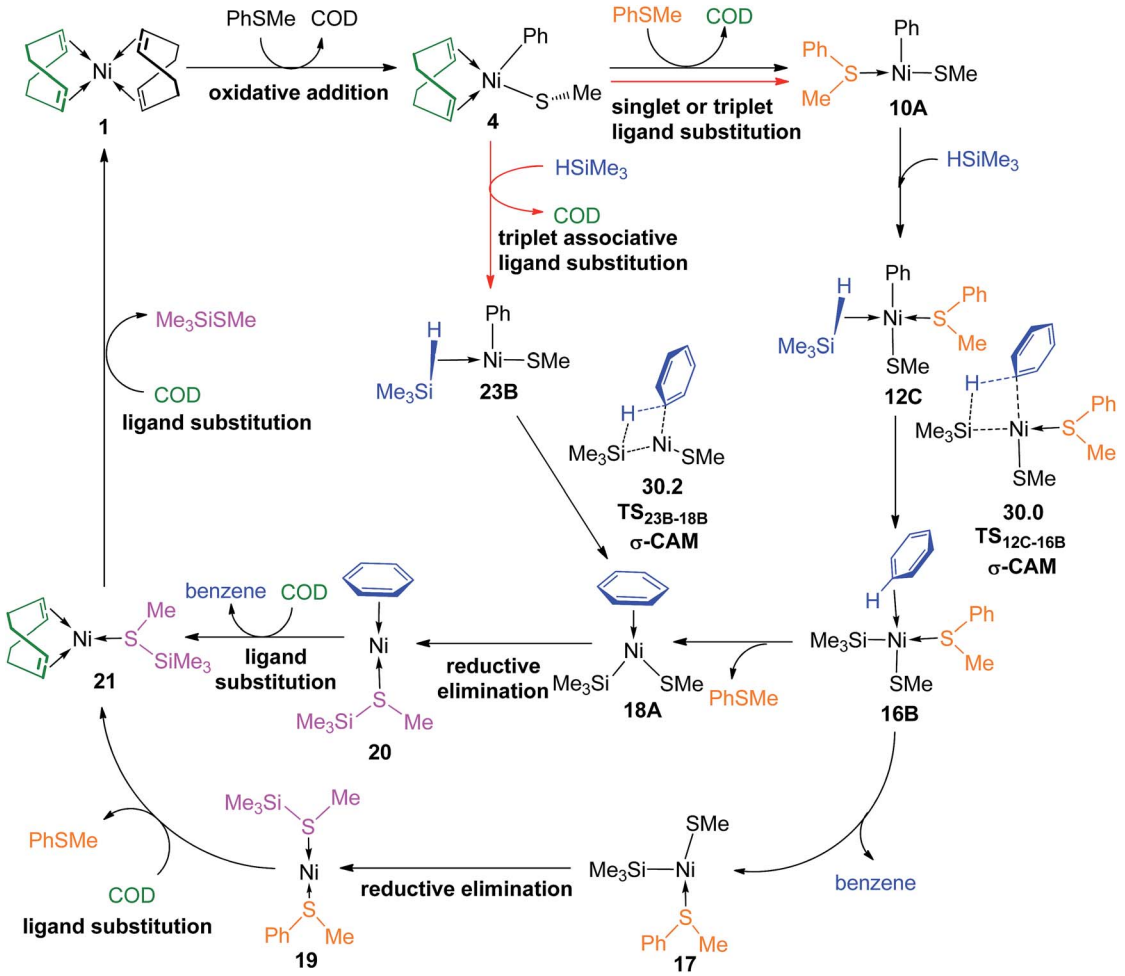

Fig. 14 The overall catalytic cycles (values of energy are given in kcal mol^{-1}).

0.3 kcal mol^{-1}. The results suggest that the PhSMe-coordianted and "ligandless" pathways are competitive. Considering the 99% yield in experiments,[15] it may be concluded that the two pathways are feasible at the early and most stages, but the "ligandless" one dominates the late stage of the reaction, as the reaction rate of PhSMe-coordinated pathway slows down when the PhSMe concentration becomes so low that there are no enough PhSMe spectator ligands.

Conclusions

The detailed reaction mechanism of $Ni(COD)_2$ catalyzed reaction of PhSMe with $HSiMe_3$ has been investigated by using density functional theory methods. The reaction mainly involves oxidative addition, ligand substitution, metathesis, reductive elimination and ligand substitution steps. For the first ligand substitution and σ-CAM, both PhSMe-coordinated pathway and "ligandless" pathway have been presented. It is found that the singlet and triplet pathways are competitive for ligand substitution of COD with PhSMe on PhSMe-coordinated pathway and that of COD with $HSiMe_3$ on "ligandless" pathway prefers the triplet mechanism. The σ-CAM transition states of these two pathways are the rate-determining TSs for the whole reaction process, with an energy difference of 0.2 (−0.3) kcal mol^{-1} at the ωB97XD/6–311++G(d,p)//B3LYP/BSI (ωB97XD/def2-QZVPPD//B3LYP/BSI) level, indicating both pathways are competitive. The competition of both pathways combined with the experimental 99% yield points out that the reaction should proceed on two pathways in early stage, as the concentration of reactant PhSMe decreases, the reaction would go on the "ligandless" reaction pathway.

Conflicts of interest

There are no conflicts to declare.

Acknowledgements

We thank the National Natural Science Foundation of China (Grants 21373098 and 21203073) for financial support. We are grateful to Computing Center of Jilin Province and High Performance Computing Center of Changchun Normal University for essential support.

Notes and references

1 J. Yamaguchi, K. Muto and K. Itami, *Top. Curr. Chem.*, 2016, **374**, 55.

2 (*a*) B. Su, Z.-C. Cao and Z.-J. Shi, *Acc. Chem. Res.*, 2015, **48**, 886–896; (*b*) Y.-Y. Gui, L. Sun, Z.-P. Lu and D.-G. Yu, *Org. Chem. Front.*, 2016, **3**, 522–526.

3 (*a*) B. M. Rosen, K. W. Quasdorf, D. A. Wilson, N. Zhang, A.-M. Resmerita, N. K. Garg and V. Percec, *Chem. Rev.*, 2011, **111**, 1346–1416; (*b*) M. Tobisu and N. Chatani, *Top. Curr. Chem.*, 2016, **374**, 41; (*c*) M. Tobisu and N. Chatani, *Acc. Chem. Res.*, 2015, **48**, 1717–1726; (*d*) T. Mesganaw and N. K. Garg, *Org. Process Res. Dev.*, 2013, **17**, 29–39.

4 (*a*) L. Hie, N. F. Nathel, T. K. Shah, E. L. Baker, X. Hong, Y.-F. Yang, P. Liu, K. N. Houk and N. K. Garg, *Nature*, 2015, **524**, 79–83; (*b*) N. A. Weires, E. L. Baker and N. K. Garg, *Nat. Chem.*, 2015, **8**, 75–79; (*c*) S. B. Blakey and D. W. C. MacMillan, *J. Am. Chem. Soc.*, 2003, **125**, 6046–6047; (*d*) X.-Q. Zhang and Z.-X. Wang, *Org. Biomol. Chem.*, 2014, **12**, 1448–1453; (*e*) M. Tobisu, K. Nakamura and N. Chatani, *J. Am. Chem. Soc.*, 2014, **136**, 5587–5590; (*f*) J. E. Dander and N. K. Garg, *ACS Catal.*, 2017, **7**, 1413–1423.

5 (*a*) K. Ishizuka, H. Seike, T. Hatakeyama and M. Nakamura, *J. Am. Chem. Soc.*, 2010, **132**, 13117–13119; (*b*) J.-Y. Chen, S.-H. Chen, X.-H. Xu, Z. Tang, C.-T. Au and R.-H. Qiu, *J. Org. Chem.*, 2016, **81**, 3246–3255; (*c*) A. Oviedo, J. Torres-Nieto, A. Arévalo and J. J. García, *J. Mol. Catal. A: Chem.*, 2008, **293**, 65–71; (*d*) J. Torres-Nieto, A. Arévalo, P. García-Gutiérrez, A. Acosta-Ramírez and J. J. García, *Ogranometallics*, 2004, **23**, 4534–4536; (*e*) J. Torres-Nieto, A. Arévalo and J. J. García, *Ogranometallics*, 2007, **26**, 2228–2233; (*f*) K. Lee, C. M. Counceller and J. P. Stambuli, *Org. Lett.*, 2009, **11**, 1457–1459.

6 F. Sondheimer and S. Wolfe, *Can. J. Chem.*, 1959, **37**, 1870–1880.

7 J. Rentner, M. Kljajic, L. Offner and R. Breinbauer, *Tetrahedron*, 2014, **70**, 8983–9027.

8 (*a*) S. Becker, Y. Fort, R. Vanderesse and P. J. Caubere, *J. Org. Chem*, 1989, **54**, 4848–4853; (*b*) J. J. Eisch, L. E. Hallenbeck and M. A. Lucarelli, *Fuel*, 1985, **64**, 440–442.

9 (*a*) H. Topsøe, B. S. Clausen and F. E. Massoth, *Hydrotreating Catalysis: Science and Technology,* Springer-Verlag, Berlin, 1996; (*b*) T. Kabe, A. Ishihara and W. Qian, *Hydrodesulfurization and Hydrodenitrogenation: Chemistry and Engineering*, Kondasa-Wiley-VCH, Tokyo, 1999.

10 (*a*) R. Mozingo, D. E. Wolf, S. A. Harris and K. Folkers, *J. Am. Chem. Soc.*, 1943, **65**, 1013–1016; (*b*) G. S. Fonken and R. Mozingo, *J. Am. Chem. Soc.*, 1947, **69**, 1212–1213; (*c*) S. A. Harris, R. Mozingo, D. E. Wolf, A. N. Wilson and K. Folkers, *J. Am. Chem. Soc.*, 1945, **67**, 2102–2106; (*d*) V. du Vigneaud, D. B. Melville, K. Folkers, D. E. Wolf, R. Mozingo, J. C. Keresztesy and S. A. Harris, *J. Biol. Chem.*, 1942, **146**, 475–485; (*e*) R. H. Billica and H. Adkins, *Org. Synth.*, 1949, **29**, 24.

11 E. Wenkert, J. M. Hanna, M. H. Leftin, E. L. Michelotti, K. T. Potes and D. Usifer, *J. Org. Chem.*, 1985, **50**, 1125–1126.

12 D. A. Vicic and W. D. Jones, *J. Am. Chem. Soc.*, 1999, **121**, 7606–7617.

13 (*a*) T. H. Graham, W. Liu and D.-M. Shen, *Org. Lett.*, 2011, **13**, 6232–6235; (*b*) T. Matsumura, T. Niwa and M. Nakada, *Tetrahedron Lett.*, 2012, **53**, 4313–4316; (*c*) T. Matsumura and M. Nakada, *Tetrahedron Lett.*, 2014, **55**, 1412–1415.

14 J. F. Hooper, R. D. Young, A. S. Weller and M. C. Willis, *Chem. - Eur. J.*, 2013, **19**, 3125–3130.

15 N. Barbero and R. Martin, *Org. Lett.*, 2012, **14**, 796–799.

16 C. Massera and G. Frenking, *Organometallics*, 2003, **22**, 2758–2765.

17 D. J. Brust and T. M. Gilbert, *Inorg. Chem.*, 2004, **43**, 1116–1121.

18 T. Sperger, I. A. Sanhueza, I. Kalvet and F. Schoenebeck, *Chem. Rev.*, 2015, **115**, 9532–9586.

19 M. J. Frisch, G. W. Trucks, H. B. Schlegel, G. E. Scuseria, M. A. Robb, J. R. Cheeseman, G. Scalmani, V. Barone, B. Mennucci, G. A. Petersson, H. Nakatsuji, M. Caricato, X. Li, H. P. Hratchian, A. F. Izmaylov, J. Bloino, G. Zheng, J. L. Sonnenberg, M. Hada, M. Ehara, K. Toyota, R. Fukuda, J. Hasegawa, M. Ishida, T. Nakajima, Y. Honda, O. Kitao, H. Nakai, T. Vreven, J. A. MontgomeryJr., J. E. Peralta, F. Ogliaro, M. Bearpark, J. J. Heyd, E. Brothers, K. N. Kudin, V. N. Staroverov, T. Keith, R. Kobayashi, J. Normand, K. Raghavachari, A. Rendell, J. C. Burant, S. S. Iyengar, J. Tomasi, M. Cossi, N. Rega, J. M. Millam, M. Klene, J. E. Knox, J. B. Cross, V. Bakken, C. Adamo, J. Jaramillo, R. Gomperts, R. E. Stratmann, O. Yazyev, A. J. Austin, R. Cammi, C. Pomelli, J. W. Ochterski, R. L. Martin, K. Morokuma, V. G. Zakrzewski, G. A. Voth, P. Salvador, J. J. Dannenberg, S. Dapprich, A. D. Daniels, O. Farkas, J. B. Foresman, J. V. Ortiz, J. Cioslowski and D. J. Fox, *Gaussian 09, Revision D.01*, Gaussian, Inc., Wallingford CT, 2013.

20 (*a*) A. D. Becke, *Phys. Rev. A*, 1988, **38**, 3098–3100; (*b*) C. Lee, W. T. Yang and R. G. Parr, *Phys. Rev. B*, 1988, **37**, 785–789; (*c*) A. D. Becke, *J. Phys. Chem.*, 1993, **98**, 5648–5652; (*d*) P. J. Stephens, F. J. Devlin, C. F. Chabalowski and M. J. Frisch, *J. Phys. Chem.*, 1994, **98**, 11623–11627; (*e*) S. H. Vosko, L. Wilk and M. Nusair, *Can. J. Phys.*, 1980, **58**, 1200–1211.

21 (*a*) K. Liu, K.-K. Liu, M.-J. Cheng and M.-H. Han, *J. Organomet. Chem.*, 2016, **822**, 1125–1126; (*b*) W. –R. Zheng, L.-L. Ding, J.-Y. Wang and Y.-X. Wang, *RSC Adv.*, 2016, **6**, 26514–26525; (*c*) X. Hong, Y. Liang and K. N. Houk, *J. Am. Chem. Soc.*, 2014, **136**, 2017–2025; (*d*) T. M. Gøgsig, J. Kleimark, S. O. Nilsson Lill, S. Korsager, A. T. Lindhardt, P.-O. Norrby and T. Skrydstrup, *J. Am. Chem. Soc.*, 2012, **134**, 443–452.

22 (*a*) A. J. H. Wachters, *J. Chem. Phys.*, 1970, **52**, 1033–1036; (*b*) P. J. Hay, *J. Chem. Phys.*, 1977, **66**, 4377–4384.

23 (*a*) J. W. McIver Jr, *J. Chem. Phys.*, 1988, **88**, 922–935; (*b*) J. W. McIver Jr, *J. Chem. Phys.*, 1990, **93**, 5634–5642.

24 J.-D. Chai and M. Head-Gordon, *Phys. Chem. Chem. Phys.*, 2008, **10**, 6615–6620.

25 A. V. Marenich, C. J. Cramer and D. G. Truhlar, *J. Phys. Chem. B*, 2009, **113**, 6378–6396.

26 M. Schlangen and H. Schwarz, *Helv. Chim. Acta*, 2008, **91**, 2203–2210.

27 A. Hellweg and D. Rappoportb, *Phys. Chem. Chem. Phys.*, 2015, **17**, 1010–1017.

28 P. Macchi, D. M. Proserpio and A. Sironi, *J. Am. Chem. Soc.*, 1998, **120**, 1447–1455.

29 M. E. Tauchert, T. R. Kaiser, A. P. V. Gçthlich, F. Rominger, D. C. M. Warth and P. Hofmann, *ChemCatChem*, 2010, **2**, 674–682.

30 R. N. Perutz and S. Sabo-Etienne, *Angew. Chem., Int. Ed.*, 2007, **46**, 2578–2592.

31 T. Nguyen, A. Panda, M. M. Olmstead, A. F. Richards, M. Stender, M. Brynda and P. P. Power, *J. Am. Chem. Soc.*, 2005, **127**, 8545–8552.

32 J. Cornella, E. Gomez-Bengoa and R. Martin, *J. Am. Chem. Soc.*, 2013, **135**, 1997–2009.

33 L.-P. Xu, L.-W. Chung and Y.-D. Wu, *ACS Catal.*, 2016, **6**, 483–493.

